SANDIA REPORT
SAND2016-5694
Unlimited Release
Printed June 2016

Simulation of Photovoltaic Power Output for Solar Integration Studies in the Southeast US

Clifford W. Hansen, Curtis Martin

Prepared by
Sandia National Laboratories
Albuquerque, New Mexico 87185 and Livermore, California 94550

Sandia National Laboratories is a multi-program laboratory managed and operated by Sandia Corporation, a wholly owned subsidiary of Lockheed Martin Corporation, for the U.S. Department of Energy's National Nuclear Security Administration under contract DE-AC04-94AL85000.

Issued by Sandia National Laboratories, operated for the United States Department of Energy by Sandia Corporation.

Available to DOE and DOE contractors from
U.S. Department of Energy
Office of Scientific and Technical Information
P.O. Box 62
Oak Ridge, TN 37831

Telephone: (865) 576-8401
Facsimile: (865) 576-5728
E-Mail: reports@adonis.osti.gov
Online ordering: http://www.osti.gov/bridge

Available to the public from
U.S. Department of Commerce
National Technical Information Service
5285 Port Royal Rd.
Springfield, VA 22161

Telephone: (800) 553-6847
Facsimile: (703) 605-6900
E-Mail: orders@ntis.fedworld.gov
Online order: http://www.ntis.gov/help/ordermethods.asp?loc=7-4-0#online

SAND2016-5694
Unlimited Release
Printed June 2016

Simulation of Photovoltaic Power Output for Integration Studies in the Southeast US

Clifford W. Hansen, Curtis Martin
Photovoltaic and Distributed Systems Integration Department
Sandia National Laboratories
P.O. Box 5800
Albuquerque, New Mexico 87185-1099

Aidan P. Tuohy
Electric Power Research Institute
942 Corridor Park Boulevard
Knoxville, TN 37902

Abstract

We describe the method used to simulate one year of AC power at one-minute intervals for a large collection of hypothetical utility-scale photovoltaic plants of varying size, employing either fixed-tilt PV modules or single-axis tracking, and for distribution-connected photovoltaic (DPV) power systems assumed for a number of metropolitan areas. We also describe the simulation of an accompanying day-ahead forecast of hourly AC power for utility-scale plants and DPV systems such that forecast errors are consistent with errors reported for current forecasting methods. The results of these simulations are intended for use in a study that examines the possible effects of increased levels of photovoltaic (PV) generation bulk on power variability within the Tennessee Valley Authority (TVA) and Southern Company service territories.

CONTENTS

FIGURES

TABLES

NOMENCLATURE

AC	alternating current
CDF	cumulative distribution function
DC	direct current
DHI	diffuse horizontal irradiance
DNI	direct normal irradiance
DOE	Department of Energy
EPRI	Electric Power Research Institute
GHI	global horizontal irradiance
mph	miles per hour
MW	megawatt
POA	plane of array
PV	photovoltaic
RMSE	root mean square error
SF	soiling factor
SNL	Sandia National Laboratories

1. INTRODUCTION

The Electric Power Research Institute (EPRI) requested Sandia National Laboratories to simulate one year of AC power output at one minute intervals from:

1. a set of hypothetical utility-scale photovoltaic plants of varying size employing a mix of fixed-tilt racking and single-axis tracking;
2. the aggregate of distribution-connected photovoltaic (DPV) power systems assumed for a number of metropolitan areas.

The results of these simulations are intended for use in a study by EPRI that examines the possible effects of increased levels of photovoltaic (PV) generation on bulk power variability within the Tennessee Valley Authority (TVA) and Southern Company service territories.

For utility-scale PV plants, EPRI provided general guidance specifying overall capacity by region. These capacity requirements were allocated among a collection of hypothetical plants of varying size which were located at sites that appeared to be geographically feasible, i.e., sufficient open space appeared to be available in the general vicinity of existing power transmission lines.

Table 1 lists the nearest community, latitude, longitude and size for each simulated plant; Figure 1 illustrates the locations chosen. Two cases were considered: a medium case with a total capacity of 10 GW AC, and an high case with 17 GW AC total capacity. In each case, 70% of the power generation capacity was assumed to be by utility-scale plants, while DPV systems provided the remaining 30%. Hence, in the medium case utility-scale plants comprised a total of 7 GW AC capacity; in the high case additional utility-scale plants were added for a total capacity of 11.9 GW AC.

For all utility-scale plants, a representative crystalline silicon module (Solar World SW175) and a representative utility-scale inverter (Siemens 1.05 MW PVS1051 inverter) were assumed. Plants were assumed to occupy 1 km^2 per 25 MW DC capacity (10 acres per MW DC). All arrays were configured for a DC to AC power ratio of 1.3 to 1 and multiple inverters were employed at a plant to provide the specified AC power output.

For both the medium and high cases, we considered each plant to comprise fixed-tilt arrays and arrays with single axis tracking. Two thirds of the capacity at each plant was modeled as mounted at a fixed tilt of 20° and an orientation of 190° and the remaining one third of capacity assumed to be mounted 20° from horizontal on single-axis horizontal roll trackers with the tracking axis oriented at 190°. Trackers were assumed to be capable of rotation to a vertical plane and to employ backtracking to avoid row-to-row shading.

For DPV, EPRI specified aggregate capacities for each metropolitan area shown in Table 2. At each metropolitan location, we assumed a mix of fixed tilt systems at different tilt and orientations as summarized in Table 3. Variation in azimuth and tilt to represent a reasonable variation in the slope and orientation of rooftops selected for solar systems. We used a simple efficiency model for DPV systems (Section 2.3) and thus no representative module or inverter is assumed.

Table 1. Location and Size of Simulated Plants.

Name	Latitude	Longitude	Elevation (m)	Capacity (MW AC)	
				Medium Case	High Case
Bowling Green, KY	36.9905	-86.5806	189	50	100
Benton, KY	36.8336	-88.3004	119	50	100
Fall Branch, TN	36.3776	-82.5880	546	100	100
Greeneville, TN	36.3464	-82.8627	447	50	50
Afton, TN	36.2300	-82.7600	515	--	100
Briceville, TN	36.1777	-84.3749	770	100	100
Heiskell, TN	36.1673	-83.9965	333	50	50
Friendsville, TN	35.7600	-84.1600	279	--	100
Gallatin, TN	36.3910	-86.5326	183	75	150
Rockvale, TN	35.7872	-86.5265	241	100	100
Murfreesboro, TN	35.8411	-86.5843	266	50	50
Readyville, TN	35.8429	-86.2053	201	--	100
Lewisburg, TN	35.6542	-86.8027	219	100	100
Columbia, TN	35.5025	-87.0935	228	50	50
Duck River, TN	35.8250	-87.3547	239	--	100
Bells, TN	35.6048	-89.0765	118	200	200
Wildersville, TN	35.8122	-88.4403	155	200	200
Henderson, TN	35.4170	-88.6508	126	100	100
Jackson, TN	35.5722	-88.7550	110	75	100
Trenton, TN	35.8980	-88.9796	118	--	200
Somerville, TN	35.3928	-89.2063	128	--	100
Milan, TN	35.9100	-88.8200	110	--	75
Lakeland, TN	35.2327	-89.6919	93	50	100
Cleveland, TN	35.1835	-84.7238	238	100	100
McDonald, TN	35.0965	-84.9963	267	50	50
Calhoun, TN	35.3600	-84.7900	268	--	100
Bull Branch, TN	35.2315	-85.2567	548	50	100
Florence, AL	34.7684	-87.8058	160	50	100
Huntsville, AL	34.4930	-86.4937	178	50	100
Guntown, MS	34.4344	-88.7524	101	200	200
Baldwyn, MS	34.4245	-88.5176	91	200	200
Nettleton, MS	34.0299	-88.6597	95	100	100
Shannon, MS	34.1647	-88.8300	82	75	75
Fulton, MS	34.2777	-88.2700	114	--	200
Smithville, MS	34.1100	-88.2800	135	--	100
West Point, MS	33.6706	-88.7902	88	200	200
W Starkville, MS	33.3916	-88.8928	94	200	200
E Starkville, MS	33.4104	-88.7357	87	100	100
Pheba, MS	33.6592	-88.9513	72	75	75
SW Pheba, MS	33.5400	-88.9800	99	--	200

Columbus MS, MS	33.5180	-88.5270	67	--	100
Tifton, GA	31.5215	-83.3636	107	450	450
Valdosta, GA	30.8235	-83.1710	57	300	300
Waycross, GA	31.1638	-82.4447	47	175	200
Albany, GA	31.4550	-84.2068	66	175	200
Bainbridge, GA	31.0014	-84.6573	42	175	200
Thomasville GA, GA	30.8940	-84.0300	61	--	300
Arlington, GA	31.3400	-84.6500	75	--	225
Nicholls, GA	31.5330	-82.7100	70	--	225
Columbus, GA	32.5786	-84.6501	150	450	450
Americus, GA	32.1753	-84.3143	147	300	300
LaGrange, GA	33.0585	-84.9216	260	175	200
Barnesville, GA	33.0458	-84.2456	243	175	200
Knoxville, GA	32.7887	-83.8487	135	175	200
Sylvester, GA	31.7280	-83.8640	97	--	300
Talbotton, GA	32.7380	-84.3230	150	--	225
Richland, GA	32.1680	-84.7320	165	--	225
Dothan, AL	31.3006	-85.5242	118	200	200
Eufaula, AL	31.9223	-85.2467	115	125	150
Opp, AL	31.2314	-86.2660	94	100	100
Brundidge, AL	31.7640	-85.7600	120	--	150
Enterprise, AL	31.2400	-85.8640	75	--	100
S Montgomery, AL	32.2241	-86.2259	71	200	200
W Montgomery, AL	32.3460	-86.5699	44	125	150
Ramer, AL	32.0180	-86.0173	150	100	100
Auburn, AL	32.6550	-85.6400	208	--	150
Selma, AL	32.4770	-87.1800	54	--	100
Atmore, AL	31.1511	-87.4557	95	200	200
Mt Vernon, AL	31.0859	-88.0627	34	125	150
Mobile, AL	30.6525	-88.3320	51	100	100
Thomasville AL, AL	31.9778	-87.7800	90	--	150
Evergreen, AL	31.5020	-86.9800	107	--	100
Jay, FL	30.7685	-87.0995	67	50	75
DeFuniak Springs, FL	30.7626	-86.2207	72	50	75
Chipley, FL	30.8051	-85.5724	33	50	75
Youngstown, FL	30.3428	-85.3003	27	50	75
Picayune, MS	30.6070	-89.7161	30	50	75
Perkinston, MS	30.6146	-89.4840	50	50	75
Vancleave, MS	30.5509	-88.8173	19	50	75
Laurel, MS	31.6906	-88.9443	88	50	75
Meridian, MS	32.4849	-88.4496	81	50	75

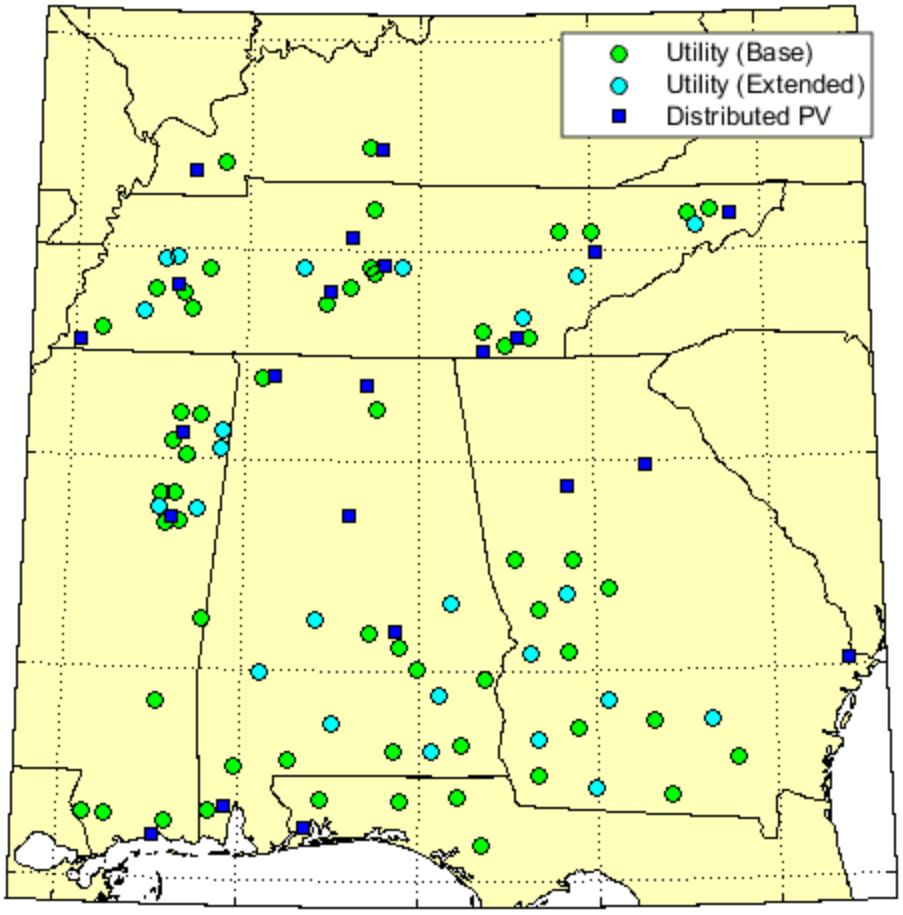

Figure 1. Map showing hypothetical PV locations.

Table 2. Summary of Distribution-Connected PV Capacities by Metro Area.

Metro Area	Latitude	Longitude	Elevation (m)	Capacity (MW AC)	
				Medium Case	High Case
Bowling Green, KY	36.9737	-86.4437	156	60	102
Mayfield, KY	36.7368	-88.6358	138	60	102
Johnson City, TN	36.3281	-82.3648	524	96	163
Knoxville, TN	35.9787	-83.9499	331	96	163
Nashville, TN	36.1171	-86.7792	162	120	204
Murfreesboro, TN	35.8644	-86.3983	185	120	204
Columbia, TN	35.6141	-87.0528	201	96	163
Jackson, TN	35.6500	-88.8293	143	24	41
Memphis, TN	35.1019	-89.9371	88	96	163
Cleveland, TN	35.1739	-84.8703	268	180	306
Chattanooga, TN	35.0406	-85.2561	255	120	204
Muscle Shoals, AL	34.7856	-87.6731	130	24	41
Huntsville, AL	34.7233	-86.6156	205	60	102
Tupelo, MS	34.2465	-88.7195	87	24	41
Starkville, MS	33.4533	-88.8187	102	24	41
Atlanta, GA	33.7717	-84.3239	290	810	1377
Savannah, GA	32.0680	-81.1732	6	324	551
Athens, GA	33.9488	-83.4127	217	180	306
Birmingham, AL	33.4710	-86.7993	213	162	275
Montgomery, AL	32.3668	-86.2691	73	54	92
Mobile, AL	30.6970	-88.1626	52	90	153
Pensacola, FL	30.4984	-87.2556	39	90	153
Biloxi, MS	30.4099	-88.9326	4	90	153

Table 3. Capacity of Distributed PV by Azimuth and Tilt Angle

	Azimuth				
Tilt	160°	170°	180°	190°	200°
15°	2%	6%	30%	9%	3%
Latitude	2%	6%	30%	9%	3%

2. METHODOLOGY

To simulate one-minute time series of AC output from each utility-scale plant, we first simulate one-minute spatially-averaged irradiance over each plant (Section 2.1), then convert irradiance to AC power using a succession of models (Section 2.2). We simulate aggregate AC power from all DPV systems in a metro region using a similar procedure (Section 2.3).We also simulate a day-ahead irradiance forecast at hourly intervals (Section 2.4) and convert the irradiance forecast to a power forecast using the same succession of models.

2.1 Simulation of One-Minute Irradiance at Utility-Scale Plants

To simulate one-minute irradiance at each plant location, we adapt a method to that was developed and applied in integration studies performed for NV Energy in 2010 [1], and for the Salt River Project Arizona in 2012 [2]. The method combines one-minute measured irradiance from ground-based sensors in the region with hourly or half-hourly irradiance measurements derived from satellite observations at each location of interest. The one-minute data is selected to be representative of the climatology at the locations of interest. The use of concurrent low-frequency data at each simulation location maintains correlations in time-averaged irradiance among locations, which is important for power system integration studies.

For this study, EPRI made available one-minute time series of measured irradiance from 25 sites at which Licor-200 instruments were deployed at roughly latitude tilt and orientation close to south. We supplement these data with one-minute time series of latitude tilt irradiance at three other sites provided by Southern Company. Figure 2 indicates the 28 sites, from which data were available between January 2012 to October 2013.

Low-frequency GHI data is estimated from half-hourly gridded values derived from GOES satellite imagery during the one-year period from November 2012 to October 2013. These estimates were produced by the University of Alabama in Huntsville and comprise down-welling shortwave global horizontal irradiance (GHI) on a grid of roughly 1km x 1km pixels at 15 and 45 minutes of each hour[1].

At each location of interest we produce a one-year time series of one minute GHI irradiance by 1) translating half-hourly GHI to a latitude tilt, 180° azimuth plane; 2) concatenating a sequence of one-day time series of one-minute latitude tilt irradiance selected from the available measured data for which half-hourly averages are similar to the translated half-hourly GHI 2) translating the one-minute time series from latitude tilt to horizontal by inverting the Erbs algorithm [3] as explained in Sect. 2.1.3.

[1] Mecikalsky, J., Development of GOES solar Insulation Datasets over TVA and Southern Company Domains, Final Report, University of Alabama in Huntsville, 9 February 2015.

2.1.1 Translation of satellite GHI to latitude tilt irradiance

We translate the half-hourly GHI to latitude tilt irradiance for each satellite pixel covered by a utility-scale plant (plants covered between 2 to 18 pixels). We make extensive use of models implemented in Sandia's PV_LIB toolbox [4] for MATLAB® to translate GHI to latitude tilt. We first calculate solar azimuth and elevation corresponding to the half-hourly sample times for each pixel using the *pvl_ephemeris.m* function. Next the solar angle of incidence (AOI) is determined using the *pvl_getaoi.m* function for fixed-tilt systems and the *pvl_singleaxis* function for single-axis tracking systems.

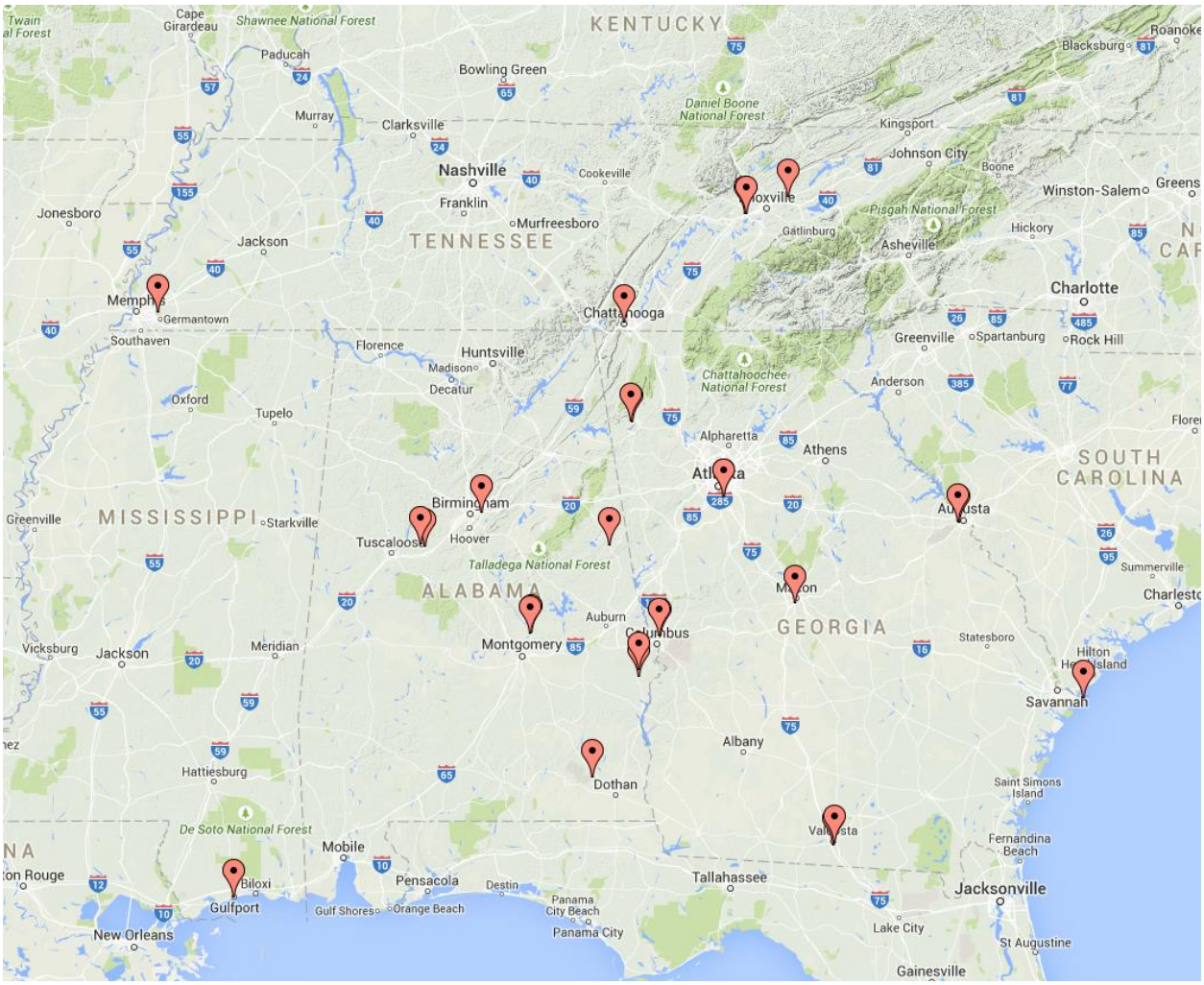

Figure 2. Locations of One-Minute Irradiance Data.

Next, we compute diffuse horizontal irradiance (DHI) from GHI using the Erbs model [3], (implemented in *pvl_erbs.m*), which we then use to calculate direct normal irradiance (DNI) using the equation

$$DNI = (GHI - DHI) / \cos(90 - SolarElevation) \quad (1).$$

The beam component of latitude tilt irradiance is then

$$E_b = DNI \cdot \cos(AOI) \quad (2).$$

We calculate the diffuse irradiance on a latitude-tilt plane, E_{diff} , as the sum of ground-reflected and sky components:

$$E_{diff} = E_{diff,ground} + E_{diff,sky} \quad (3) .$$

The ground-reflected component, $E_{diff,ground}$, is calculated using a simple geometric model (implemented in *pvl_grounddiffuse.m*) that assumes the ground is horizontal and uniformly reflective ([5], Eq. 22.38):

$$E_{diff,ground} = \rho \cdot GHI \cdot \frac{1-\cos\beta}{2} \quad (4),$$

where β is the tilt angle relative to horizontal and it is assumed that the ground albedo $\rho = 0.2$. The sky component, $E_{diff,sky}$, is calculated using an empirical model developed by J. Hay and J. Davies [6] (implemented in *pvl_haydavies1980.m*).

Latitude tilt irradiance at each pixel location is the sum of the three components:

$$G_{POA} = E_b + E_{diff,sky} + E_{diff,ground} \quad (5).$$

We average these time series across the pixels included in a plant to obtain a half-hourly time series of latitude-tilt irradiance for each plant. This half-hourly time series provide the reference for constructing a one year time series of one-minute latitude tilt irradiance for each plant.

2.1.2 Downscaling from Half-Hourly to One-Minute Irradiance

We construct simulated one-minute time series of latitude-tilt irradiance at each plant location one day at a time. For each calendar month, we assemble a library of daily one-minute latitude-tilt irradiance profiles from the ground-measured one-minute latitude tilt irradiance data and computed half-hourly averages over windows centered at 15 and 45 minutes of each hour. Then, for each day of the calendar month, we select from the library a one-minute irradiance profile for each simulated plant. We select the profile that minimizes the sum of the squared differences between the half-hourly satellite and ground data. This daily selection process is done without replacement to avoid using the same one-minute irradiance profile at different plants on the same calendar day. To avoid biasing the simulated irradiance, we consider the plants in a random order on each calendar day. For each location, we concatenate the sequence of selected one-minute profiles to form a year-long time series of one-minute latitude tilt irradiance.

2.1.3 Converting from latitude tilt irradiance to GHI

We use a numerical technique suggested by Yang et al. [7] to invert from latitude tilt irradiance to GHI. Using the Erbs model [3] for diffuse horizontal irradiance DHI and the Hay model (Eq. A.5 in [7]) for the diffuse transposition factor R_d, latitude tilt irradiance G_{POA} can be written as a function of the global horizontal transmittance K_t. Starting with Eq. (5)

$$G_{POA} = DNI\cos\left(AOI\right) + DHI \times R_d + \rho \times GHI \times \frac{1-\cos\beta}{2} \tag{6}$$

We write I_0 for extraterrestrial normal irradiance, $K_n = DNI/I_0$ for direct irradiance transmittance, $DF = DHI/GHI$ for the diffuse fraction, $K_d = K_t - K_n$ for the diffuse transmittance and Z for solar zenith angle. From

$$K_t = \frac{GHI}{I_0\cos Z} \tag{7}$$

we obtain $K_n = \left(1-DF\right)K_t$ which leads to

$$\begin{aligned} G_{POA} &= I_0 K_n \cos\left(AOI\right) + DF \times GHI \times R_d + \rho \times GHI \times \frac{1-\cos\beta}{2} \\ &= I_0\left(1-DF\right)K_t\cos\left(AOI\right) + DF \times I_0 K_t \cos Z \times R_d + \rho \times I_0 K_t \cos Z \times \frac{1-\cos\beta}{2} \end{aligned} \tag{8}$$

The Erbs model [3] comprises an empirical function $DF = DF\left(K_t\right)$. The Hay model (Eq. A.5, [7]) provides R_d:

$$R_d = K_d\frac{\cos\left(AOI\right)}{\cos Z} + \left(1-K_d\right)\frac{1+\cos\beta}{2} \tag{9}$$

Algebraic manipulation yields

$$\begin{aligned} G_{POA} &= I_0\left(1-DF\right)K_t\cos\left(AOI\right) + DF \times I_0 K_t \cos Z \times R_d + \rho \times I_0 K_t \cos Z \times \frac{1-\cos\beta}{2} \\ &= I_0 K_t\left[\left(1-DF+DF^2K_t\right)\cos\left(AOI\right) + \left(DF\left(1-DF\times K_t\right)\frac{1+\cos\beta}{2} + \rho\frac{1-\cos\beta}{2}\right)\cos Z\right] \end{aligned} \tag{10}$$

which comprises a polynomial in K_t after the substitution $DF = DF\left(K_t\right)$.

At each time sample we determine a value for K_t that minimizes the difference between G_{POA} (Eq. (10)) and latitude-tilt irradiance. We then compute GHI by Eq. (7).

2.1.4 Determining Spatial Average Irradiance

Even though the time series of one-minute GHI is developed using spatially averaged half-hourly GHI values as a reference, the one-minute GHI values are derived from one-minute latitude-tilt irradiance measured using a point sensor. Output from a PV plant correlates with the spatial aggregate irradiance over the entire plant footprint, rather than to irradiance at a point within or near the plant [8]. Consequently, spatially averaged irradiance over each plant's footprint must be determined. We estimate the spatial average GHI at each minute by using a simple moving average of the one-minute time series of GHI, where the duration of the averaging window was equal to the number of minutes it would take for a cloud to completely traverse a square plant of the required capacity, assuming that each plant would yield 25 MW per square kilometer. Using a numerical weather model [9], we estimate daily cloud speeds v at each plant location for the time period of interest. The length of the averaging window, T, is then given by $T = \sqrt{A}/v$, where A represents the area of the plant.

2.2 Conversion of Irradiance to Power

Conversion of GHI to power first requires decomposing the spatially-averaged, one minute GHI into direct and diffuse irradiance components and translating these components to the array's plane, to arrive at plane-of-array (POA) irradiance. We use the Erbs model [3] to estimate DHI from GHI and compute $DNI = (GHI - DHI)/\cos Z$. We translate DNI and DHI to the POA by using the Hay and Davies model [6]. For fixed tilt arrays, the array plane is at 20° tilt and 190° azimuth; for arrays with single-axis tracking, the array plane is computed using *pvl_singleaxis.m* with assumptions of horizontal roll trackers oriented at 190° azimuth and 20° tilt.

Sandia's Array Performance Model (SAPM) [10] and Inverter Models [11] were used to compute AC power for each plant. SAPM simulates the DC output of PV modules. Inputs to SAPM (implemented in *pvl_sapm.m*) include a set of module parameters for the representative module which were determined previously from outdoor testing, effective irradiance E_e (the irradiance converted to DC current in the modules), and cell temperature. We estimate effective irradiance in suns as $E_e = POA/E_0$ where $E_0 = 1000\ \mathrm{W/m^2}$ is a unit conversion factor. We neglect the relatively small effects on E_e of the spectral content of POA irradiance and of reflections from the array surface. Both of these effects are most pronounced at low sun elevations and are important when accuracy of power modeling is the primary goal. In this analysis, we judged that simulating power without these effects would still reasonably represent the magnitude and variability of the simulated power over the fleet of hypothetical plants.

We calculate cell temperature from ambient temperature T_a and surface wind speed WS using [10]

$$T_{cell} = T_m + E_e \cdot \Delta T\ , \tag{11}$$

$$T_m = T_a + \exp(a + bWS) \tag{12}$$

where T_m represents the temperature on the module back surface, $\Delta T = 3°\text{C}$ is the difference in temperature between a module's back surface and a cell at an irradiance level of 1000w/m^2, and *a* and *b* are empirical constants determined from outdoor testing of the representative module. For each plant we obtained hourly measurements of T_a and wind speed *WS* from data from the nearest weather station cataloged in NOAA's Integrated Surface Database [12], and linearly interpolated these data to obtain one-minute time series.

By feeding the simulated DC voltage and current produced by SAPM into the Sandia inverter model (*pvl_snlinverter.m*) with parameters specific to the Siemens PVS1051 inverter, we obtain AC power for a single inverter at each plant. The single-inverter AC output is multiplied by the number of inverters to obtain AC output for the entire plant.

2.3 Calculation of Power from Distribution-Connected PV Systems

Power from the DPV systems is calculated by applying the methods outlined in Sect. 2.1 to obtain the estimated spatial average GHI irradiance in each pixel within each metropolitan area. Next, using the GHI time series data from each of these pixels, we apply the methods described in Section 2.2 to compute POA irradiance for each azimuth and tilt combination detailed in Table 3. Using the weights given in Table 3, we then compute a weighted average POA for each pixel. Finally, we average these time series across all the included pixels to produce a spatial and system average POA for each metropolitan area. The use of a single spatial average is appropriate because we assume that each class of DPV system is randomly distributed across each metropolitan area.

We obtain ambient temperature and wind speed time series by linearly interpolating hourly measurements from the weather station cataloged in NOAA's Integrated Surface Database [12] closest to each metropolitan center. Using generic values from [10] for the *a* and *b* parameters in Eq. (12) we compute cell temperature. Finally, we obtained a time series for the AC power from each metropolitan area from the formula

$$P_{AC} = P_{DC} \cdot 0.81 \cdot \frac{POA}{E_0} \cdot \left[1 - 0.005\left(T_{cell} - 25\right)\right] ,$$

where P_{DC} represents the DC power capacity for each area specified in Table 2. The factor 0.81 represents a roll-up of all the efficiencies involved in the sunlight-to-AC power conversion chain, while the factor in brackets represents the effect of ambient temperature on AC power.

2.4 Simulation of Day-Ahead Hourly Forecast Power

For unit commitment and dispatch modeling, time series of forecast power production are required. We simulate day-ahead forecasts at hourly intervals for each simulated plant using the algorithm developed for the integration study performed for NV Energy [1]. The algorithm

stochastically generates a relative forecast error for each hour of the year, and the forecast irradiance is obtained by multiplying each hour's average simulated irradiance by the relative forecast error. Forecast errors are generated using the algorithm developed for the NV Energy integration study [1]. The forecast errors are generated differently on clear and cloudy days, consistent with the forecast methods described by Lorenz et al. [13]. For each clear day, the relative error is determined by a single normally distributed random variable with mean of one and standard deviation of 0.05. For cloudy days, forecast errors are determined for each hour using normally distributed random variables with standard deviation depending on the hour's clear-sky index value (i.e., the hourly average GHI divided by the average hourly GHI from a clear-sky model, in this analysis, the Ineichen model [14]). Lorenz et al. report relative RMSE conditional on various bins of the clear-sky index ([13], Fig. 5).

Day-ahead forecasts of hourly temperature and wind speed are simulated by a simple persistence forecast based on the recorded temperature and wind speed for each location. For the first day, the forecast temperature and wind speed were assumed equal to the measured values at each site. For successive days in the calendar, the forecast values are equal to the measured values for the preceding day.

A day-ahead forecast of AC power is then obtained from the day-ahead forecasts of irradiance, temperature and wind speed by repeating the steps outlined in Sect. 2.1 and Sect. 2.2. Because the relative forecast error is applied to hourly-averaged irradiance, no spatial smoothing is applied.

4. REFERENCES

1. Hansen, C.W., J. S. Stein, A. Ellis, *Simulation of One-Minute Power Output from Utility-Scale Photovoltaic Generation Systems*, SAND Report 2011-5529, Sandia National Laboratories, Albuquerque, NM, 2011.
2. Hansen, C.W., A. Luketa-Hanlin, A.P. Tuohy, and K. M. Nicole, *Simulation of Photovoltaic Power Output for the Salt River Project Integration Study*, SAND Report 2012-9920, Sandia National Laboratories, Albuquerque, NM, 2012.
3. D.G. Erbs, S.A. Klein and J.A.Duffie, "Estimation of the diffuse radiation fraction for hourly, daily and monthly-average global radiation," *Solar Energy*, vol. 28, pp. 293-302, 1982.
4. Sandia National Laboratories (SNL), PV_Lib toolbox for MATLAB, retrieved from http://pvpmc.org/pv-lib/, May 2015.
5. Lorenzo, E., *Energy Collected Delivered by PV Modules*, in Photovoltaic Science and Engineering 2nd ed., eds. A. Luque and S. Hegedus, Wiley 2011.
6. Loutzenhiser P.G., et al., "Empirical validation of models to compute solar irradiance on inclined surfaces for building energy simulation," *Solar Energy*, vol. 81, pp. 254-267, 2007.
7. Yang, D., et al., "Evaluation of transposition and decomposition models for converting global solar irradiance from tilted surface to horizontal in tropical regions," *Solar Energy*, vol. 97, pp. 369-387, 2013.
8. Kuszmaul, S., A. Ellis, J. Stein, L. Johnson, *Lanai High-Density Irradiance Sensor Network for Characterizing Solar Resource Variability of MW-Scale PV System*, Proc. of the 35th IEEE Photovoltaic Specialist Conference, Honolulu, HI, 2010.
9. Lave, Matthew and Jan Kleissl, "Cloud speed impact on solar variability scaling – Application to the wavelet variability model," *Solar Energy*, vol. 91, pp. 11-21, 2013.
10. King, David L., W. E. Boyson, J. A. Kratochvil, *Photovoltaic Array Performance Model*, SAND2004-3535, Sandia National Laboratories, Albuquerque, NM, August 2004.
11. King, David L., S. Gonzalez, G. M. Galbraith, W. E. Boyson, *Performance Model for Grid-Connected Photovoltaic Inverters*, SAND2007-5036, Sandia National Laboratories, Albuquerque, NM, September 2007.
12. National Oceanic and Atmospheric Administration National Centers for Environmental Information, *Integrated Surface Database*, retrieved from https://www.ncdc.noaa.gov/isd, November 2014.
13. Lorenz, E., *Irradiance Forecasting for the Power Prediction of Grid-Connected Photovoltaic Systems*, IEEE Jour. of Sel. Topics in Appl. Earth Obs. And Remote Sensing, Vol 2 pp. 2-10, Mar. 2009.
14. Ineichen, P., and R. Perez, "A new airmass independent formulation for the Linke turbidity coefficient," *Solar Energy*, vol. 73, pp. 151-157, 2002.

DISTRIBUTION

1	Electric Power Research Institute (electronic copy) Attn: Mr. Aidan Tuohy 942 Corridor Park Boulevard Knoxville, TN 37902		
1	MS0115	OFA/NFE Agreements	10112
1	MS0899	Technical Library	9536 (electronic copy)


Sandia National Laboratories